Intermittency in an optomechanical cavity near a subcritical Hopf bifurcation

Oren Suchoi,[1] Lior Ella,[2] Oleg Shtempluk,[2] and Eyal Buks[2,*]

[1]*Russell Berrie Nanotechnology Institute, Technion, Haifa 32000, Israel*

[2]*Department of Electrical Engineering, Technion, Haifa 32000, Israel*

(Received 2 June 2014; revised manuscript received 22 July 2014; published 11 September 2014)

We experimentally study an optomechanical cavity consisting of an oscillating mechanical resonator embedded in a superconducting microwave transmission line cavity. Tunable optomechanical coupling between the mechanical resonator and the microwave cavity is introduced by positioning a niobium-coated single-mode optical fiber above the mechanical resonator. The capacitance between the mechanical resonator and the coated fiber gives rise to optomechanical coupling, which can be controlled by varying the fiber-resonator distance. We study radiation-pressure-induced self-excited oscillation as a function of microwave driving parameters (frequency and power). Intermittency between limit-cycle and steady-state behaviors is observed with blue-detuned driving frequency. The experimental results are accounted for by a model that takes into account the Duffing-like nonlinearity of the microwave cavity. A stability analysis reveals a subcritical Hopf bifurcation near the region where intermittency is observed.

DOI: 10.1103/PhysRevA.90.033818 PACS number(s): 42.50.Pq, 05.45.−a, 46.40.Ff, 62.40.+i

I. INTRODUCTION

The field of cavity optomechanics [1–4] deals with a family of systems, each composed of two coupled elements. The first one is a mechanical resonator, commonly having a low damping rate, and the second one is an electromagnetic cavity, which typically is externally driven. Both radiation pressure [5–13] and bolometric force [14–24] can give rise to the coupling between the mechanical resonator and the cavity. In recent years a variety of cavity optomechanical systems have been constructed and studied [3,5,6,7,8,11,13,19,25–34], and phenomena such as mode cooling [25,33–36], self-excited oscillation [6,14,18,20,28,32,37–39], and optically induced transparency [40–43] have been investigated. In addition to applications in metrology [44,45] and photonics [46–48], optomechanical cavities may allow the experimental study of the transition from the classical realm to the quantum one [31,33,49–66]. While much experimental and theoretical progress has been made in reaching the ground state and observing the linear dynamics of mechanical objects, it is becoming appreciated that nonlinearity allows the creation of nonclassical mechanical states [56] and can be exploited for improving the efficiency of optomechanical cooling [67]. It is therefore important to study and shed light on the nonlinear dynamics of these devices.

In this work we experimentally study self-excited oscillation in an optomechanical cavity operating in the microwave band. We introduce a method for achieving strong and tunable optomechanical coupling, which is based on positioning a metallically coated optical fiber near the mechanical resonator. The microwave cavity, which is made of a superconducting aluminum microstrip, exhibits Kerr-type nonlinearity [68–71], which significantly affects the dynamics of the entire optomechanical system [67]. The response of the system to a monochromatic pump signal that is injected into the microwave cavity is investigated. Self-excited oscillation is observed in a certain region in the plane of the of drive parameters (pump frequency and pump power). We find that a good agreement between the experimental results and theory can be obtained provided that cavity nonlinearity is taken into account [67]. In a certain region of drive parameters the system exhibits random jumps between a limit cycle (i.e., self-excited oscillation) and a fixed point. A theoretical stability analysis reveals that this observed intermittency behavior occurs near a subcritical [57,72–74] Hopf bifurcation [56,63].

II. EXPERIMENTAL SETUP

The experimental setup is schematically depicted in Fig. 1. Magnetron dc sputtering is employed for coating a high-resistivity silicon wafer with aluminum. The aluminum layer is annealed *in situ* at 400 °C for 10–30 min to reduce internal stress in the layer [75]. A standard photolithography process is used to pattern the microwave microstrip cavity. At the open end of the microstrip a 100-nm-thick SiN membrane is fabricated [23]. The mechanical resonator is made by releasing a $100 \times 100\ \mu\mathrm{m}^2$ trampoline supported by four beams using electron cyclotron resonance (ECR) dry etch. At the other end the cavity is weakly coupled to a feed line, which guides both the injected and reflected microwave signals. The results presented here are obtained with a device that has a fundamental cavity resonance frequency $\omega_a/2\pi = 2.5465$ GHz, cavity linear damping rate $\gamma_a/2\pi = 420$ kHz, fundamental mechanical resonance frequency $\omega_b/2\pi = 12.1$ kHz, and mechanical linear damping rate $\gamma_b/2\pi = 1.63$ Hz.

As can be seen in Fig. 1, a single-mode optical fiber coated with niobium is placed above the suspended trampoline. In the presence of the coated fiber two optomechanical cavities are formed, one in the microwave band and the other in the optical band [23]. The fact that both optomechanical cavities share the same mechanical resonator can be exploited for conversion between microwave and optical photons [76–82]. However, in the present work we employ the optical cavity and the optical setup seen in Fig. 1 only for fiber positioning and for characterization of the mechanical resonator at high temperatures, whereas all low-temperature measurements

*Corresponding author: eyal@ee.technion.ac.il

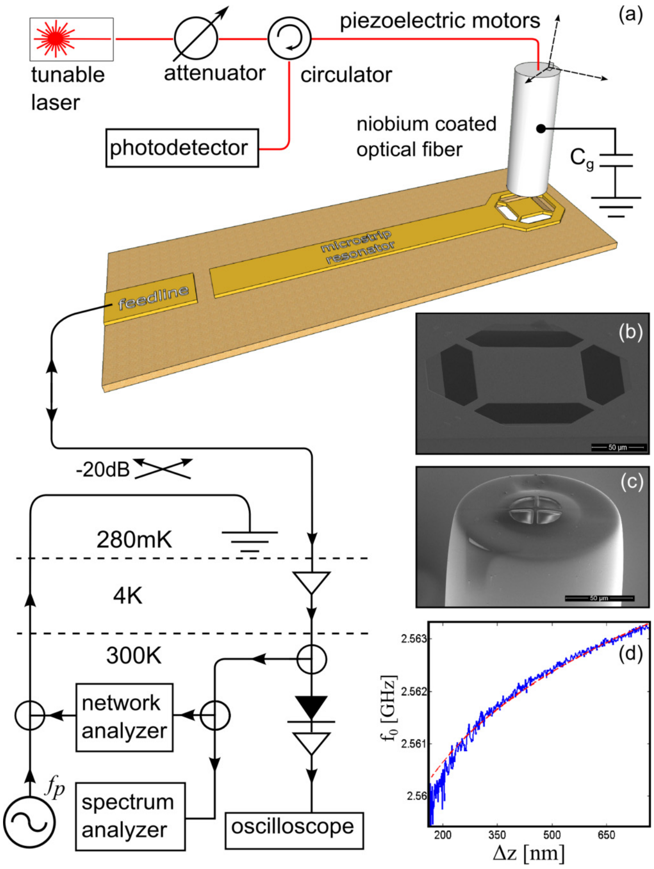

FIG. 1. (Color online) (a) Experimental setup. The microwave cavity is a microstrip made of aluminum over high-resistivity silicon wafer coated with a 100-nm-thick SiN layer. The mechanical resonator at the end of the microstrip is a suspended trampoline supported by four beams. (b) Electron micrograph of the trampoline. The optomechanical coupling is generated using a niobium-coated optical fiber that is positioned at submicron distance from the trampoline. (c) Several windows are opened in the niobium layer on the fiber tip using FIB. The optical setup (seen above the sample) allows using the optical fiber for displacement detection, whereas the microwave setup (seen below the sample) is employed for measuring the cavity response. The coated fiber is galvanically connected to both ac and dc voltage sources with a bias-T (not seen in the sketch), which can be used to externally actuate the mechanical resonator. The sample is mounted inside a closed copper package, which is internally coated with niobium. Measurements are performed in a dilution refrigerator operating at a temperature of 0.28 K and in vacuum. (d) The measured (solid) and calculated (dashed) cavity resonance frequency f_0 vs fiber-trampoline distance Δz.

that are discussed below are done in the microwave band only.

We employ a telecom single-mode optical fiber with a fiber Bragg grating (FBG) mirror [23] and a focusing lens made by melting the fiber tip. Magnetron dc sputtering is used for coating the fiber with niobium. To allow optical transmission, we etch the niobium coating using a focused ion beam (FIB), thus exposing the core of the fiber at the tip. A cryogenic piezoelectric three-axis positioning system with subnanometer resolution is employed to manipulate the position of the optical fiber.

III. OPTOMECHANICAL COUPLING

Optomechanical coupling between the microwave cavity and the mechanical resonator is introduced due to the capacitance between the coated fiber and the suspended trampoline, which is approximately given by $C_{\mathrm{SP}} = 2\pi\epsilon_0 R_{\mathrm{F}} \ln(R_{\mathrm{F}}/\Delta z)$ [83], where $R_{\mathrm{F}} = 350\ \mu$m is the radius of curvature of the melted fiber tip, Δz is the fiber-trampoline distance, and ϵ_0 is the vacuum permittivity. A hole of diameter $d_{\mathrm{H}} = 2.4$ mm and depth $h_{\mathrm{H}} = 2.7$ mm is drilled in the sample package, which is made of copper, above the trampoline in order to allow inserting the optical fiber, which has an outer diameter of $d_{\mathrm{F}} = 125\ \mu$m. When the fiber is centered inside the hole, the fiber-package coaxial capacitance is given by $C_{\mathrm{g}} = 2\pi\epsilon_0 h_{\mathrm{H}}/\ln(d_{\mathrm{H}}/d_{\mathrm{F}})$ [84]. When radiation loss is disregarded, the effect of the coated fiber on microwave cavity modes can be accounted for by assuming that a termination with purely imaginary impedance given by $Z_{\mathrm{T}} = 1/i\omega C$, where $C^{-1} = C_{\mathrm{SP}}^{-1} + C_{\mathrm{g}}^{-1}$, has been introduced between the microstrip end and the ground. The frequencies f_a of the cavity modes can be found by solving $\tan(\kappa l_{\mathrm{M}}) = i Z_0/Z_{\mathrm{T}}$ [84], where the propagation constant κ is related to f_a by $f_a = \kappa c'/2\pi$, c' is the propagation velocity in the microstrip, l_{M} is the length of the microstrip, and $Z_0 = 48\ \Omega$ is its characteristic impedance. A comparison between the measured and calculated values of the cavity fundamental mode frequency f_0 is seen in Fig. 1(d). The dependence of f_0 on fiber-trampoline distance Δz allows the extraction of the optomechanical coupling coefficient Ω, which is found to be given by $\Omega/x_{b0} = 55$ MHz $\mu\mathrm{m}^{-1}$ for our chosen operating point, where $x_{b0} = \sqrt{\hbar/2m\omega_b}$ is the mechanical zero-point amplitude and where $m = 5.4 \times 10^{-12}$ kg is the effective mass of the mechanical mode.

IV. RESULTS

The microwave cavity is excited by injecting a monochromatic pump signal with frequency $f_{\mathrm{p}} = \omega_{\mathrm{p}}/2\pi$ and amplitude b_{p} into the feed line and monitoring the off-reflected signal using either a spectrum analyzer or a diode connected to an oscilloscope [see Fig. 1(a)]. The amplitude b_{p} is related to the pump power P_{p} by $P_{\mathrm{p}} = \hbar\omega_a |b_{\mathrm{p}}|^2$. In the absence of any optomechanical coupling (i.e. when the fiber is positioned far from the trampoline) the cavity reflectivity exhibits bistability in a certain region in the plane of pump parameters (frequency f_{p} and amplitude b_{p}) as a result of cavity Kerr nonlinearity. The border line of this region contains a cusp point, which is also known as the onset of bistability point [71]. The values of pump frequency and pump amplitude at that critical point are labeled by $f_{\mathrm{c}} = \omega_{\mathrm{c}}/2\pi$ and b_{c}, respectively [see Eqs. (A26) and (A27)]. In what follows we employ normalized and dimensionless parameters for the pump detuning $\Delta/\Delta_{\mathrm{c}} = (\omega_{\mathrm{p}} - \omega_a)/|\omega_{\mathrm{c}} - \omega_a|$ and for the pump amplitude $b_{\mathrm{p}}/b_{\mathrm{c}}$.

Figures 2(a) and 2(b) show the reflected microwave power, which is measured using a spectrum analyzer, at frequency $f_{\mathrm{p}} - f_b$, where $f_b = \omega_b/2\pi$ is the mechanical resonance frequency, for both forward and backward sweeps of the pump frequency f_{p}. A strong peak is found at frequency $f_{\mathrm{p}} - f_b$ [as well as at other harmonics $f_{\mathrm{p}} + n f_b$, where n is an integer, as can be seen in Fig. 3(a)] in a certain region in the

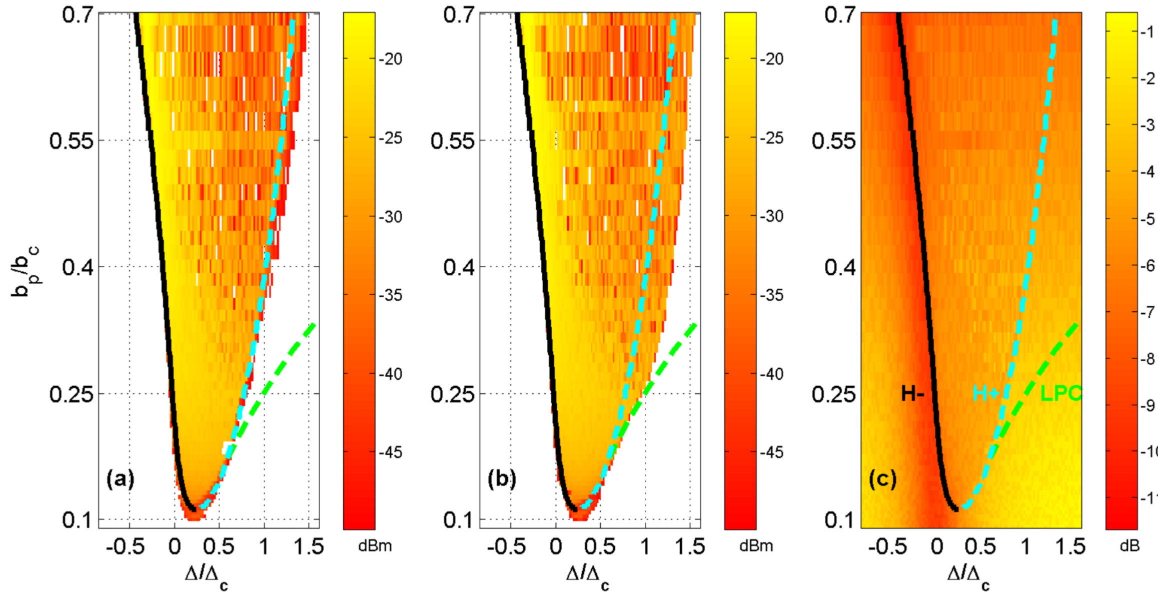

FIG. 2. (Color online) Self-excited oscillation. The reflected power at angular frequency $\omega_p - \omega_b$ for (a) backward and (b) forward frequency sweeps. The pump critical power is $P_c = -19.5$ dB m, and the pump critical detuning is $\Delta_c = -2\pi \times 0.7$ MHz. (c) The reflected power at angular frequency ω_p. The solid black, dotted cyan, and dotted green lines represent, respectively, supercritical Hopf (labeled H_-), subcritical Hopf (labeled H_+), and limit point of cycle bifurcations (labeled LPC). The following cavity parameters are employed for the bifurcation calculation: $K_a/\omega_a = -1.44 \times 10^{-15}$ and $\gamma_{a3}/K_a = 0.04$.

plane of normalized pump parameters Δ/Δ_c and b_p/b_c, inside which self-excited oscillation occurs. The height of the peak at frequency $f_p - f_b$ is plotted in Figs. 2(a) and 2(b). The results obtained with backward sweep [Fig. 2(a)] differ from those obtained with forward sweep [Fig. 2(b)], which indicates that the cavity response is hysteretic due to bistability. Figure 2(c) depicts the reflected power at f_p.

The data presented in Fig. 2 cannot be theoretically accounted for unless cavity nonlinearity is taken into account. For example, when cavity nonlinearity is disregarded, self-excited oscillation is expected to occur only with blue detuning [see Eq. (A31)], whereas the data in Figs. 2(a) and 2(b) demonstrate a self-excited oscillation with both blue and red detuning (at sufficiently high pump power). Furthermore, while the cavity reflectivity is expected to be power independent when cavity nonlinearity is disregarded [see Eq. (A34)], the data in Fig. 2(c) clearly show pulling in the frequency response due to the cavity Kerr nonlinearity.

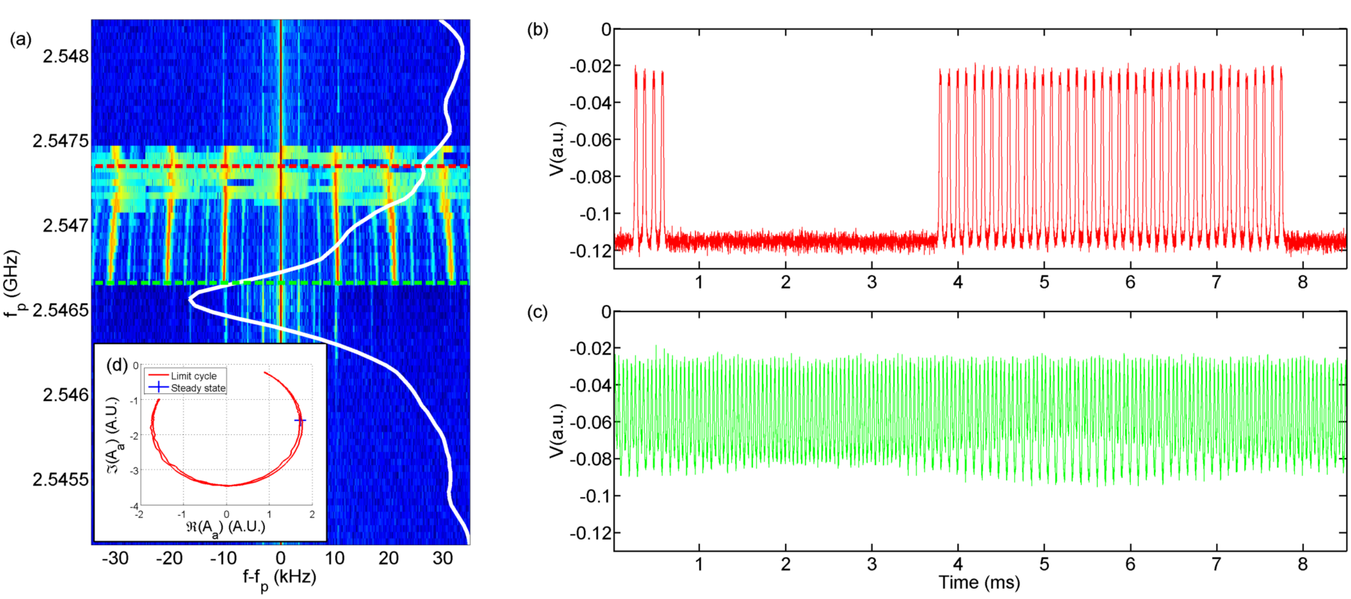

FIG. 3. (Color online) Intermittency. (a) The measurement of the reflected signal using a spectrum analyzer. (b) and (c) The time traces measured using an oscilloscope for two values of f_p, which are indicated in (a) by the two dashed lines. The solid white line in (a) shows the reflected power at the pump frequency f_p. Noise-induced transitions between a limit cycle and a fixed point are seen in (b). (d) The projection of the limit cycle (red line) and the fixed point (blue cross) on the complex A_a plane.

To take into account cavity Kerr nonlinearity [69,85] the theoretical modeling of Refs. [67,86] is employed. The Hamiltonian of the optomechanical system is taken to be given by Eq. (A1) in the Appendix. The cavity nonlinear response is characterized by the Kerr nonlinearity coefficient K_a and nonlinear damping rate γ_{a3}. The equations of motion of the system in the rotating frame of the driven cavity are given by Eqs. (A14) and (A15). Fixed points of the equations of motion are found by solving Eq. (A20). Note that for the region seen in Fig. 2 the fixed point is unique (since $b_{\mathrm{p}}/b_{\mathrm{c}} < 1$). The stability of the fixed points is determined by linearization of the equations of motion [see Eq. (A30)] and by calculating the eigenvalues of the Jacobian matrix of the linearized equations.

V. STABILITY ANALYSIS

Stability analysis of the linearized equations of motion can determine the stability of fixed points. However, further analysis is needed in order to identify limit-cycle solutions and to determine their stability. To that end we employ the numerical continuation package MATCONT [87] in order to identify bifurcations and to construct the stability map of the system in the plane of pump parameters. The solid black, dotted cyan, and dotted green lines in Fig. 2 represent, respectively, supercritical Hopf (labeled H_-), subcritical Hopf (labeled H_+), and limit point of cycle (LPC) bifurcations. In the numerical investigation noise is disregarded, and the operators are treated as c numbers. The cavity parameters that are used for the numerical calculation are listed in the caption of Fig. 2. The bifurcation lines divide the region in the plane of pump parameters seen in Fig. 2 into three zones. In the zone between the H_- and H_+ bifurcations only a single limit cycle is found to be locally stable (although the existence of other locally stable solutions cannot be ruled out); in the zone between the H_+ and LPC bifurcations bistability of a limit cycle and a locally stable fixed point occurs, whereas elsewhere only a unique fixed point is found.

Intermittency, i.e., random jumps between the limit cycle and the fixed point, is experimentally observed for $b_{\mathrm{p}}/b_{\mathrm{c}} > 0.2$. Figure 3 shows frequency and time-domain measurements taken with a normalized pump amplitude given by $b_{\mathrm{p}}/b_{\mathrm{c}} = 0.58$. Figure 3(a) shows the frequency decomposition of the reflected signal as the pump frequency f_{p} is scanned, and the white line shows the reflected power at frequency f_{p}. Regular self-excited oscillation in the time domain can be seen in Fig. 3(c) for normalized detuning $\Delta/\Delta_{\mathrm{c}} = 0.2$. At larger detuning $\Delta/\Delta_{\mathrm{c}} = 1.5$ (in the bistable zone), however, random transitions between the limit cycle and the fixed point occur, as can be seen in Fig. 3(b). The limit cycle and the fixed point in the complex A_a projection plane of phase space are plotted in Fig. 3(d). Note that the dynamics near the fixed point remains relatively slow even when it becomes locally unstable (i.e., in the zone between the H_- and H_+ bifurcations). Consequently, in the presence of noise even a locally unstable fixed point can give rise to intermittency-like behavior provided that it is sufficiently close to the limit cycle. Indeed, intermittency is experimentally observed on both sides of the H_+ bifurcation.

VI. CONCLUSION

In summary, we find that a subcritical Hopf bifurcation is the underlying mechanism that is responsible for the experimentally observed intermittency. While the current study is focused on the classical dynamics, future study will explore the possibility of exploiting dynamical bistability for the creation of macroscopic nonclassical states of the optomechanical system [88].

ACKNOWLEDGMENTS

This work was supported by the Israel Science Foundation, the binational science foundation, the Security Research Foundation in the Technion, the Israel Ministry of Science, the Russell Berrie Nanotechnology Institute, the European STREP QNEMS Project, and MAFAT. The authors thank Y. Schneider for helping in sample fabrication.

APPENDIX: OPTOMECHANICAL CAVITY

In this Appendix, which is based on Ref. [86], the equations of motion for the optomechanical cavity are derived. Nonlinearity in the response of the microwave cavity is taken into account to lowest nonvanishing order. Fixed-point solutions are derived, and their stability is analyzed. Analytical results are obtained for the case where cavity nonlinearity can be disregarded.

1. The model

The Hamiltonian $\mathcal{H}$ of the optomechanical cavity is taken to be given by

$$\begin{aligned}
\mathcal{H} = {} & \hbar\omega_a N_a + \frac{\hbar}{2} K_a A_a^\dagger A_a^\dagger A_a A_a + \hbar\omega_b N_b \\
& + \hbar\Omega N_a (A_b + A_b^\dagger) \\
& + \hbar \int d\omega\, a_{a1}^\dagger(\omega)\, a_{a1}(\omega)\, \omega \\
& + \hbar \int d\omega\, [T_{a1} A_a^\dagger a_{a1}(\omega) + T_{a1}^* a_{a1}^\dagger(\omega) A_a] \\
& + \hbar \int d\omega\, a_{a2}^\dagger(\omega)\, a_{a2}(\omega)\, \omega \\
& + \hbar \int d\omega\, [T_{a2} A_a^\dagger a_{a2}(\omega) + T_{a2}^* a_{a2}^\dagger(\omega) A_a] \\
& + \hbar \int d\omega\, a_{a3}^\dagger(\omega)\, a_{a3}(\omega)\, \omega \\
& + \hbar \int d\omega\, [T_{a3} A_a^\dagger A_a^\dagger a_{a3}(\omega) + T_{a3}^* a_{a3}^\dagger(\omega) A_a A_a] \\
& + \hbar \int d\omega\, a_b^\dagger(\omega)\, a_b(\omega)\, \omega \\
& + \hbar \int d\omega\, [T_b A_b^\dagger a_b(\omega) + T_b^* a_b^\dagger(\omega) A_b],
\end{aligned} \tag{A1}$$

where A_a, $A_a^\dagger$, and $N_a = A_a^\dagger A_a$ (A_b, $A_b^\dagger$, and $N_b = A_b^\dagger A_b$) are, respectively, annihilation, creation, and number operators of the microwave cavity (mechanical resonator), denoted as a (denoted as b). Kerr-like nonlinearity of the driven microwave cavity is taken into account to lowest order by including the term $(\hbar/2)K_a A_a^\dagger A_a^\dagger A_a A_a$. Due to the dispersive optomechanical coupling, which is described by the term $\hbar\Omega N_a(A_b + A_b^\dagger)$, the effective resonance frequency of the microwave cavity becomes linearly dependent on the displacement of the mechanical resonator, which is proportional to $A_b + A_b^\dagger$. The microwave cavity is coupled to three semi-infinite transmission lines. The first, denoted as $a1$, is a feed line, which is linearly coupled to the cavity with a coupling constant $T_{a1} = \sqrt{\gamma_{a1}/\pi}e^{i\phi_{a1}}$ and which is employed to deliver the input and output signals; the second, denoted as $a2$, is linearly coupled to the microwave cavity with a coupling constant $T_{a2} = \sqrt{\gamma_{a2}/\pi}e^{i\phi_{a2}}$, and it is used to model linear dissipation, whereas the third one, denoted as $a3$, is nonlinearly coupled to the microwave cavity with a coupling constant $T_{a3} = \sqrt{\gamma_{a3}/2\pi}e^{i\phi_{a3}}$ and is employed to model nonlinear dissipation. Linear damping of the mechanical resonator is modeled using the semi-infinite transmission line, which is denoted as b and which is linearly coupled to the mechanical resonator with a coupling constant $T_b = \sqrt{\gamma_b/\pi}e^{i\phi_b}$. All damping rates ($\gamma_{a1}$, γ_{a2}, γ_{a3}, and γ_b) are positive and all phase factors (ϕ_{a1}, ϕ_{a2}, ϕ_{a3}, and ϕ_b) are real.

The superconducting kinetic inductance is the main underlying mechanism responsible for the Kerr-like nonlinearity. Associated with the kinetic inductance is the nonlinear resistance of the two-photon absorptive type. These nonlinear effects are relatively strong in superconducting strip lines and microstrips due to the nonuniform distribution of the microwave current along the cross section of the transmission line. Along the edges, where the current density obtains its peak value, the current density can become overcritical even with relatively moderate power levels. As a result, the superconducting current density may vary, and consequently, both inductance L and resistance R per unit length become current dependent according to the form [69]

$$L = L_0 + \Delta L\left(\frac{I}{I_c}\right)^2, \tag{A2}$$

$$R = R_0 + \Delta R\left(\frac{I}{I_c}\right)^2, \tag{A3}$$

where I (I_c) is the total (critical) current. The values of ΔL and ΔR together with the mode waveform of the microwave cavity allow the calculation of the coefficients K_a and γ_{a3}, respectively [71].

2. Equations of motion

The Heisenberg equation of motion for the cavity operator A_a is given by

$$\begin{aligned}\frac{dA_a}{dt} &= -i\omega_a A_a - iK_a N_a A_a - i\Omega A_a(A_b + A_b^\dagger)\\ &\quad - i\int d\omega\, T_{a1}a_{a1}(\omega) - i\int d\omega\, T_{a2}a_{a2}(\omega)\\ &\quad - 2i\int d\omega\, T_{a3}A_a^\dagger a_{a3}(\omega),\end{aligned} \tag{A4}$$

and that for the mechanical resonator operator A_b is given by

$$\frac{dA_b}{dt} = -i\omega_b A_b - i\Omega N_a - i\int d\omega\, T_b a_b(\omega)\ . \tag{A5}$$

Integrating the equations of motion for the bath operators $a_{a1}(\omega)$, $a_{a2}(\omega)$, $a_{a3}(\omega)$, and $a_b(\omega)$ and substituting the results into Eqs. (A4) and (A5) yield

$$\begin{aligned}\frac{dA_a}{dt} &= -[i\omega_a + \gamma_a + (iK_a + \gamma_{a3})N_a]A_a - i\Omega A_a(A_b + A_b^\dagger)\\ &\quad - i\sqrt{2\gamma_{a1}}e^{i\phi_{a1}}a_{a1}^{\text{in}}(t) - i\sqrt{2\gamma_{a2}}e^{i\phi_{a2}}a_{a2}^{\text{in}}(t)\\ &\quad - 2i\sqrt{\gamma_{a3}}e^{i\phi_{a3}}A_a^\dagger a_{a3}^{\text{in}}(t),\end{aligned} \tag{A6}$$

$$\frac{dA_b}{dt} = -(i\omega_b + \gamma_b)A_b - i\Omega N_a - i\sqrt{2\gamma_b}e^{i\phi_b}a_b^{\text{in}}(t), \tag{A7}$$

where

$$\gamma_a = \gamma_{a1} + \gamma_{a2}, \tag{A8}$$

the input operator $a_{a1}^{\text{in}}(t)$ is given by

$$a_{a1}^{\text{in}}(t) = \frac{1}{\sqrt{2\pi}}\int d\omega\, a_{a1}(\omega,t_0)\, e^{i\omega(t_0 - t)}, \tag{A9}$$

the time t_0 is assumed to be in the distant past, and similar expressions define the other input operators $a_{a2}^{\text{in}}(t)$, $a_{a3}^{\text{in}}(t)$, and $a_b^{\text{in}}(t)$.

Consider the case where a coherent tone at angular frequency ω_p and a constant complex amplitude b_p is injected into the feed line. The operators of the driven cavity and its thermal baths are expressed in a frame rotating at frequency ω_p as

$$a_{a1}^{\text{in}} = b_p e^{-i\omega_p t} + c_{a1}^{\text{in}}e^{-i\omega_p t}, \tag{A10}$$

$$a_{a2}^{\text{in}} = c_{a2}^{\text{in}}e^{-i\omega_p t}, \tag{A11}$$

$$a_{a3}^{\text{in}} = c_{a3}^{\text{in}}e^{-i\omega_p t}, \tag{A12}$$

$$A_a = C_a e^{-i\omega_p t}. \tag{A13}$$

With this notation Eqs. (A6) and (A7) can be rewritten as

$$\frac{dC_a}{dt} + \Theta_a = F_a, \tag{A14}$$

$$\frac{dA_b}{dt} + \Theta_b = F_b, \tag{A15}$$

where

$$\begin{aligned}\Theta_a &= \Theta_a(C_a, C_a^\dagger, A_b, A_b^\dagger)\\ &= \{i[-\Delta + \Omega(A_b + A_b^\dagger)] + \gamma_a + (iK_a + \gamma_{a3})N_a\}C_a\\ &\quad + i\sqrt{2\gamma_{a1}}e^{i\phi_{a1}}b_p,\end{aligned} \tag{A16}$$

$\Delta = \omega_p - \omega_a$ is the drive frequency detuning,

$$\Theta_b = \Theta_b(C_a, C_a^\dagger, A_b, A_b^\dagger) = (i\omega_b + \gamma_b)A_b + i\Omega N_a, \tag{A17}$$

and the noise terms F_a and F_b are given by

$$\begin{aligned}F_a &= -i\sqrt{2\gamma_{a1}}e^{i\phi_{a1}}c_{a1}^{\text{in}} - i\sqrt{2\gamma_{a2}}e^{i\phi_{a2}}c_{a2}^{\text{in}}\\ &\quad - 2i\sqrt{\gamma_{a3}}e^{i(\phi_{a3} + \omega_p t)}C_a^\dagger c_{a3}^{\text{in}}\end{aligned} \tag{A18}$$

and

$$F_b = -i\sqrt{2\gamma_b} e^{i\phi_b} a_b^{\text{in}}(t) . \tag{A19}$$

3. Fixed points

Fixed points are found by solving

$$\Theta_a(B_a,B_a^*,B_b,B_b^*) = \Theta_b(B_a,B_a^*,B_b,B_b^*) = 0, \tag{A20}$$

where both B_a and B_b are considered to be complex numbers. With the help of Eqs. (A16) and (A17) one finds that

$$\left[\left(-\Delta + K_a^{\text{eff}} E_a\right)^2 + (\gamma_a + \gamma_{a3} E_a)^2\right] E_a = 2\gamma_{a1}|b_{\text{p}}|^2, \tag{A21}$$

where $E_a = |B_a|^2$ and where

$$K_a^{\text{eff}} = K_a - \frac{2\Omega^2 \omega_b}{\omega_b^2 + \gamma_b^2} . \tag{A22}$$

Finding E_a by solving Eq. (A21) allows calculating B_a using the relation

$$\left\{-i\Delta + \gamma_a + \left(iK_a^{\text{eff}} + \gamma_{a3}\right)|B_a|^2\right\} B_a + i\sqrt{2\gamma_{a1}} e^{i\phi_{a1}} b_{\text{p}} = 0 \tag{A23}$$

and B_b using the relation

$$(i\omega_b + \gamma_b) B_b + i\Omega |B_a|^2 = 0 . \tag{A24}$$

4. Onset of bistability point

When b_{p} is sufficiently large, the response of the system becomes bistable; that is, E_a becomes a multivalued function of cavity detuning Δ in some range near the resonance. The onset of the bistability point is defined as the point for which $\partial\Delta/\partial E_a = 0$ and $\partial^2\Delta/\partial (E_a)^2 = 0$. Such a point occurs only if the nonlinear damping is sufficiently small [71], namely, only when the following condition holds:

$$\left|K_a^{\text{eff}}\right| > \sqrt{3}\gamma_{a3}. \tag{A25}$$

At the onset of the bistability point the drive frequency detuning Δ_{c}, the pump amplitude b_{c}, and the cavity number of photons E_{c} are given by

$$\Delta_{\text{c}} = \gamma_a \frac{K_a^{\text{eff}}}{\left|K_a^{\text{eff}}\right|} \left[\frac{4\gamma_{a3}\left|K_a^{\text{eff}}\right| + \sqrt{3}\left[\left(K_a^{\text{eff}}\right)^2 + \gamma_{a3}^2\right]}{\left(K_a^{\text{eff}}\right)^2 - 3\gamma_{a3}^2}\right], \tag{A26}$$

$$b_{\text{c}}^2 = \frac{4}{3\sqrt{3}} \frac{\gamma_a^3\left[\left(K_a^{\text{eff}}\right)^2 + \gamma_{a3}^2\right]}{\gamma_{a1}\left(\left|K_a^{\text{eff}}\right| - \sqrt{3}\gamma_{a3}\right)^3}, \tag{A27}$$

$$E_{\text{c}} = \frac{2\gamma_a}{\sqrt{3}\left(\left|K_a^{\text{eff}}\right| - \sqrt{3}\gamma_{a3}\right)}. \tag{A28}$$

5. Linearization

To study fluctuation near the fixed points the solution is expressed as

$$C_a = B_a + c_a, \tag{A29a}$$

$$A_b = B_b + c_b, \tag{A29b}$$

where both operators c_a and c_b are considered to be small. The linearized equations of motion can be written in a matrix form as [see Eqs. (A14) and (A15)]

$$\frac{d}{dt}\begin{pmatrix} c_a \\ c_a^\dagger \\ c_b \\ c_b^\dagger \end{pmatrix} + W \begin{pmatrix} c_a \\ c_a^\dagger \\ c_b \\ c_b^\dagger \end{pmatrix} = \begin{pmatrix} F_a \\ F_a^\dagger \\ F_b \\ F_b^\dagger \end{pmatrix}, \tag{A30}$$

where $W = \partial(\Theta_a,\Theta_a^*,\Theta_b,\Theta_b^*)/\partial(B_a,B_a^*,B_b,B_b^*)$ is the Jacobian matrix [see Eqs. (A16) and (A17)].

The four eigenvalues of W are labeled as λ_{a1}, λ_{a2}, λ_{b1}, and λ_{b2}. In the limit $\Omega \to 0$, i.e., when the mechanical resonator is decoupled from the cavity, it is assumed that λ_{a1} and λ_{a2} become the eigenvalues of the decoupled cavity and λ_{b1} and λ_{b2} become the eigenvalues of the decoupled mechanical resonator. In general a fixed point is locally stable provided that all eigenvalues of W have a positive real part. Typically, in optomechanical cavities stability is lost when the real parts of the mechanical eigenvalues λ_{b1} and λ_{b2} simultaneously vanish. At that point Hopf bifurcation occurs, and a limit cycle is born. The bifurcation can be either supercritical or subcritical, depending on the sign of the first Lyapunov coefficient, which is proportional to the additive inverse of the effective nonlinear damping of the mechanical resonator. Bistability of the fixed point and the limit cycle occurs in a certain range of parameters when the bifurcation is subcritical, whereas no such bistability occurs when the bifurcation is supercritical.

The statistical properties of the noise operators F_a and F_b are calculated by assuming that all bath modes are in thermal equilibrium at temperature T. It is found that F_a and F_b are uncorrelated and that both expectation values $\langle F_a\rangle$ and $\langle F_b\rangle$ vanish. Moreover, the power spectrums S_a of the noise term F_a are found to be given by $S_a = \pi^{-1}\Gamma_a(1 - e^{-\beta\hbar\omega_a})^{-1}$, where $\beta = 1/k_{\text{B}}T$, k_{B} is Boltzmann's constant, and $\Gamma_a = \gamma_a + 2\gamma_{a3}\langle N_a\rangle$, and the power spectrums S_b of the noise term F_b is found to be given by $S_b = \pi^{-1}\gamma_b(1 - e^{-\beta\hbar\omega_b})^{-1}$.

6. Disregarding cavity nonlinearity

When the number of cavity photons E_a is sufficiently small, cavity nonlinearity can be disregarded. Furthermore, when the coupling constant Ω can be considered to be small, the eigenvalues of the Jacobian matrix W can be analytically evaluated to second order in Ω using perturbation theory. The result for the mechanical eigenvalue $\lambda_{b1} = \lambda_{b2}^*$ for the case $\gamma_b \ll \omega_b$ is given by

$$\lambda_{b1} = i\omega_b + \gamma_b + \frac{2\Omega^2 E_a}{\omega_b}\Xi_1(d,g), \tag{A31}$$

where

$$\begin{aligned}\Xi_l(d,g) &= \frac{1}{-i(d+l)+g} - \frac{1}{-i(-d+l)+g} \\ &= \frac{-4dlg - 2id(l^2 - d^2 - g^2)}{[(l+d)^2 + g^2][(l-d)^2 + g^2]},\end{aligned} \tag{A32}$$

$d = \Delta_a^{\text{eff}}/\omega_b$ is the dimensionless detuning, $\Delta_a^{\text{eff}} = \Delta - \Omega(B_b + B_b^*)$ is the effective detuning, and $g = \gamma_a/\omega_b$ is the dimensionless cavity damping. Note that for this case Hopf bifurcation can occur only in the region of blue detuning; that is, the condition $\text{Re}\lambda_{b1} = 0$ can be satisfied only when $d > 0$.

When cavity nonlinearity is disregarded, the number of cavity photons E_a is given by [see Eq. (A21)]

$$E_a = \frac{2\gamma_{a1}|b_{\mathrm{p}}|^2}{\left(\Delta_a^{\mathrm{eff}}\right)^2 + \gamma_a^2}. \tag{A33}$$

When the fixed point is locally stable, the cavity reflectivity r_a for the same case is given by

$$r_a = \frac{i\,\Delta_a^{\mathrm{eff}} + \gamma_{a1} - \gamma_{a2}}{i\,\Delta_a^{\mathrm{eff}} - \gamma_{a1} - \gamma_{a2}}. \tag{A34}$$

[1] V. B. Braginskiĭ and A. B. Manukin, Sov. Phys. JETP **25**, 653 (1967).
[2] F. Marquardt and S. M. Girvin, Physics **2**, 40 (2009).
[3] T. J. Kippenberg and K. J. Vahala, Science **321**, 1172 (2008).
[4] F. Marquardt and S. M. Girvin, arXiv:0905.0566.
[5] O. Arcizet, P.-F. Cohadon, T. Briant, M. Pinard, and A. Heidmann, Nature (London) **444**, 71 (2006).
[6] T. Carmon, H. Rokhsari, L. Yang, T. J. Kippenberg, and K. J. Vahala, Phys. Rev. Lett. **94**, 223902 (2005).
[7] T. Corbitt, Y. Chen, E. Innerhofer, H. Müller-Ebhardt, D. Ottaway, H. Rehbein, D. Sigg, S. Whitcomb, C. Wipf, and N. Mavalvala, Phys. Rev. Lett. **98**, 150802 (2007).
[8] S. Gigan, H. R. Böhm, M. Paternostro, F. Blaser, J. B. Hertzberg, K. C. Schwab, D. Bauerle, M. Aspelmeyer, and A. Zeilinger, Nature (London) **444**, 67 (2006).
[9] A. M. Jayich, J. C. Sankey, B. M. Zwickl, C. Yang, J. D. Thompson, S. M. Girvin, A. A. Clerk, F. Marquardt, and J. G. E. Harris, New J. Phys. **10**, 095008 (2008).
[10] E. F. Nichols and G. F. Hull, Phys. Rev., Ser. I **13**, 307 (1901)
[11] A. Schliesser, P. Del'Haye, N. Nooshi, K. J. Vahala, and T. J. Kippenberg, Phys. Rev. Lett. **97**, 243905 (2006).
[12] A. Schliesser, R. Riviere, G. Anetsberger, O. Arcizet, and T. J. Kippenberg, Nat. Phys. **4**, 415 (2008).
[13] J. D. Thompson, B. M. Zwickl, A. M. Jayich, F. Marquardt, S. M. Girvin, and J. G. E. Harris, Nature (London) **452**, 72 (2008).
[14] K. Aubin, M. Zalalutdinov, T. Alan, R. B. Reichenbach, R. Rand, A. Zehnder, J. Parpia, and H. Craighead, J. Microelectromech. Syst. **13**, 1018 (2004).
[15] G. Jourdan, F. Comin, and J. Chevrier, Phys. Rev. Lett. **101**, 133904 (2008).
[16] S. De Liberato, N. Lambert, and F. Nori, Phys. Rev. A **83**, 033809 (2011).
[17] F. Marino and F. Marin, Phys. Rev. E **83**, 015202(R) (2011).
[18] F. Marquardt, J. G. E. Harris, and S. M. Girvin, Phys. Rev. Lett. **96**, 103901 (2006).
[19] C. H. Metzger and K. Karrai, Nature (London) **432**, 1002 (2004).
[20] C. Metzger, M. Ludwig, C. Neuenhahn, A. Ortlieb, I. Favero, K. Karrai, and F. Marquardt, Phys. Rev. Lett. **101**, 133903 (2008).
[21] M. Paternostro, S. Gigan, M. S. Kim, F. Blaser, H. R. Böhm, and M. Aspelmeyer, New J. Phys. **8**, 107 (2006).
[22] J. Restrepo, J. Gabelli, C. Ciuti, and I. Favero, C. R. Phys. **12**, 860 (2011).
[23] S. Zaitsev, A. K. Pandey, O. Shtempluck, and E. Buks, Phys. Rev. E **84**, 046605 (2011).
[24] S. Zaitsev, O. Gottlieb, and E. Buks, Nonlinear Dyn. **69**, 1589 (2012).
[25] J. Chan, T. P. M. Alegre, A. H. Safavi-Naeini, J. T. Hill, A. Krause, S. Gröblacher, M. Aspelmeyer, and O. Painter, Nature (London) **478**, 89 (2011).
[26] T. Corbitt and N. Mavalvala, J. Opt. B **6**, S675 (2004).
[27] S. Gröblacher, J. T. Hill, A. H. Safavi-Naeini, J. Chan, and O. Painter, Appl. Phys. Lett. **103**, 181104 (2013).
[28] K. Hane and K. Suzuki, Sens. Actuators A **51**, 179 (1996).
[29] C. Metzger, I. Favero, S. Camerer, D. Konig, H. Lorenz, J. P. Kotthaus, and K. Karrai, Appl. Phys. Lett. **90**, 104101 (2007).
[30] D. Kleckner and D. Bouwmeester, Nature (London) **444**, 75 (2006).
[31] A. D. O'Connell, M. Hofheinz, M. Ansmann, Radoslaw C. Bialczak, M. Lenander, E. Luceroand, M. Neeley, D. Sank, H. Wang, M. Weides, J. Wenner, J. M. Martinis, and A. N. Cleland, Nature (London) **464**, 697 (2010).
[32] C. A. Regal, J. D. Teufel, and K. W. Lehnert, Nat. Phys. **4**, 555 (2008).
[33] J. D. Teufel, D. Li, M. S. Allman, K. Cicak, A. J. Sirois, J. D. Whittaker, and R. W. Simmonds, Nature (London) **471**, 204 (2011).
[34] J. D. Teufel, T. Donner, D. Li, J. W. Harlow, M. S. Allman, K. Cicak, A. J. Sirois, J. D. Whittaker, K. W. Lehnert, and R. W. Simmonds, Nature (London) **475**, 359 (2011).
[35] S. Gröblacher, J. B. Hertzberg, M. R. Vanner, G. D. Cole, S. Gigan, K. C. Schwab, and M. Aspelmeyer, Nat. Phys. **5**, 485 (2009).
[36] A. Schliesser, O. Arcizet, R. Rivière, G. Anetsberger, and T. J. Kippenberg, Nat. Phys. **5**, 509 (2009).
[37] T. Carmon and K. J. Vahala, Phys. Rev. Lett. **98**, 123901 (2007).
[38] T. Corbitt, D. Ottaway, E. Innerhofer, J. Pelc, and N. Mavalvala, Phys. Rev. A **74**, 021802 (2006).
[39] K. Kim and S. Lee, J. Appl. Phys. **91**, 4715 (2002).
[40] M. Karuza, C. Biancofiore, M. Bawaj, C. Molinelli, M. Galassi, R. Natali, P. Tombesi, G. Di Giuseppe, and D. Vitali, Phys. Rev. A **88**, 013804 (2013).
[41] T. Ojanen and K. Borkje, Phys. Rev. A **90**, 013824 (2014).
[42] A. H. Safavi-Naeini, T. P. Mayer Alegre, J. Chan, M. Eichenfield, M. Winger, Q. Lin, J. T. Hill, D. E. Chang, and O. Painter, Nature (London) **472**, 69 (2011).
[43] S. Weis, R. Riviere, S. Deleglise, E. Gavartin, O. Arcizet, A. Schliesser, and T. J. Kippenberg, Science **330**, 1520 (2010).
[44] V. B. Braginsky and F. Ya. Khalili, *Quantum Measurement* (Cambridge University Press, Cambridge, 1995).
[45] A. A. Clerk, M. H. Devoret, S. M. Girvin, F. Marquardt, and R. J. Schoelkopf, Rev. Mod. Phys. **82**, 1155 (2010).
[46] M. Bagheri, M. Poot, M. Li, W. P. H. Pernice, and H. X. Tang, Nat. Nanotechnol. **6**, 726 (2011).
[47] M. Hossein-Zadeh and K. J. Vahala, IEEE J. Sel. Top. Quantum Electron. **16**, 276 (2010).
[48] X. Zhou, F. Hocke, A. Schliesser, A. Marx, H. Huebl, R. Gross, and T. J. Kippenberg, Nat. Phys. **9**, 179 (2013).
[49] M. Bahrami, M. Paternostro, A. Bassi, and H. Ulbricht, Phys. Rev. Lett. **112**, 210404 (2014).

[50] A. Farace, F. Ciccarello, R. Fazio, and V. Giovannetti, Phys. Rev. A **89**, 022335 (2014).
[51] C. Galland, N. Sangouard, N. Piro, N. Gisin, and T. J. Kippenberg, Phys. Rev. Lett. **112**, 143602 (2014).
[52] C. Genes, D. Vitali, P. Tombesi, S. Gigan, and M. Aspelmeyer, Phys. Rev. A **77**, 033804 (2008).
[53] Q. Y. He and M. D. Reid, Phys. Rev. A **88**, 052121 (2013).
[54] S. Kiesewetter, Q. Y. He, P. D. Drummond, and M. D. Reid, arXiv:1312.6474.
[55] H. J. Kimble, Y. Levin, A. B. Matsko, K. S. Thorne, and S. P. Vyatchanin, Phys. Rev. D **65**, 022002 (2001).
[56] N. Lörch, J. Qian, A. Clerk, F. Marquardt, and K. Hammerer, Phys. Rev. X **4**, 011015 (2014).
[57] C. P. Meaney, R. H. McKenzie, and G. J. Milburn, Phys. Rev. E **83**, 056202 (2011).
[58] T. A. Palomaki, J. D. Teufel, R. W. Simmonds, and K. W. Lehnert, Science **342**, 710 (2013).
[59] I. Pikovski, M. R Vanner, M. Aspelmeyer, M. S. Kim, and Č. Brukner, Nat. Phys. **8**, 393 (2012).
[60] M. Poot and H. S. J. van der Zant, Phys. Rep. **511**, 273 (2012).
[61] J. Qian, A. A. Clerk, K. Hammerer, and F. Marquardt, Phys. Rev. Lett. **109**, 253601 (2012).
[62] D. A. Rodrigues and A. D. Armour, Phys. Rev. Lett. **104**, 053601 (2010).
[63] S. Walter, A. Nunnenkamp, and C. Bruder, Phys. Rev. Lett. **112**, 094102 (2014).
[64] A. J. Weinstein, C. U. Lei, E. E. Wollman, J. Suh, A. Metelmann, A. A. Clerk, and K. C. Schwab, arXiv:1404.3242.
[65] X.-W. Xu, H. Wang, J. Zhang, and Y. Liu, Phys. Rev. A **88**, 063819 (2013).
[66] X. Xu, M. Gullans, and J. M. Taylor, arXiv:1404.3726.
[67] P. D. Nation, M. P. Blencowe, and E. Buks, Phys. Rev. B **78**, 104516 (2008).
[68] K. Børkje, A. Nunnenkamp, J. D. Teufel, and S. M. Girvin, Phys. Rev. Lett. **111**, 053603 (2013).
[69] T. Dahm and D. J. Scalapino, J. Appl. Phys. **81**, 2002 (1997).
[70] O. Suchoi, B. Abdo, E. Segev, O. Shtempluck, M. P. Blencowe, and E. Buks, Phys. Rev. B **81**, 174525 (2010).
[71] B. Yurke and E. Buks, J. Lightwave Technol. **24**, 5054 (2006).
[72] D. Blocher, R. H. Rand, and A. T. Zehnder, Int. J. Non-Linear Mech. **52**, 119 (2013).
[73] C. A. Holmes, C. P. Meaney, and G. J. Milburn, Phys. Rev. E **85**, 066203 (2012).
[74] J. Larson and M. Horsdal, Phys. Rev. A **84**, 021804 (2011).
[75] V. P. Jaecklin, C. Linder, J. Brugger, N. F. de Rooij, J.-M. Moret, and R. Vuilleumier, Sens. Actuators A **43**, 269 (1994).
[76] R. W. Andrews, R. W. Peterson, T. P. Purdy, K. Cicak, R. W. Simmonds, C. A. Regal, and K. W. Lehnert, Nat. Phys. **10**, 321 (2014).
[77] J. Bochmann, A. Vainsencher, D. D. Awschalom, and A. N. Cleland, Nat. Phys. **9**, 712 (2013).
[78] K. Y. Fong, L. Fan, L. Jiang, X. Han, and H. X. Tang, arXiv:1404.3427.
[79] C. Jiang, Y. Cui, H. Liu, and G. Chen, arXiv:1404.3928.
[80] L. Tian, Ann. Phys. 1 (2014).
[81] B. D. Clader, Phys. Rev. A **90**, 012324 (2014).
[82] Z. Yin, W. L. Yang, L. Sun, and L. M. Duan, arXiv:1407.4938.
[83] A. Russel, Proc. Phys. Soc. London **35**, 10 (1922).
[84] D. M. Pozar, *Microwave Engineering* (Wiley, New York, 1998).
[85] E. A. Tholen, A. Ergul, E. M. Doherty, F. M. Weber, F. Gregis, and D. B. Haviland, Appl. Phys. Lett. **90**, 253509 (2007).
[86] E. Buks, C. R. Phys. **13**, 454 (2012).
[87] MATCONT, http://www.matcont.ugent.be.
[88] A. D. Armour and D. A. Rodrigues, C. R. Phys. **13**, 440 (2012).